UNIVERSITY OF BIRMINGHAM

Research at Birmingham

Synthesis, structural and magnetic characterisation of the fluorinated compound 15R-BaFeO2F

Clemens, Oliver; Berry, Frank; Bauer, Jessica; Wright, Adrian; Knight, Kevin S.; Slater, Peter

Document Version
Publisher's PDF, also known as Version of record

Link to publication on Research at Birmingham portal

Synthesis, structural and magnetic characterisation of the fluorinated compound 15R-BaFeO$_2$F

Oliver Clemens [a],*, Frank J. Berry [a], Jessica Bauer [b], Adrian J. Wright [a], Kevin S. Knight [c], Peter R. Slater [a]

[a] School of Chemistry, The University of Birmingham, Birmingham B15 2TT, United Kingdom
[b] Anorganische Festkörperchemie, Universität des Saarlandes, Am Markt, Zeile 3, 66125 Saarbrücken, Germany
[c] ISIS Facility, Rutherford Appleton Laboratory, Harwell Oxford, Didcot OX11 0QX, United Kingdom

ABSTRACT

The compounds 15R-BaFeO$_2$F and 15R-BaFeO$_{2.27}$F$_{0.5}$ have been synthesised by the low temperature fluorination of 15R-BaFeO$_{3-d}$F$_{0.2}$ using polyvinylidenedifluoride (PVDF) as a fluorination agent. The materials have been structurally characterised by Rietveld analysis of the X-ray- and HRPD-powder neutron diffraction data. A detailed analysis of bond valence sums suggests that the oxide and fluoride ions order on the different anion sites. A reinvestigation of our recently published structure (Clemens et al., 2013) [34] of 6H-BaFeO$_2$F is also reported and incorporation of fluoride in h-type layers is also confirmed in this compound. The magnetic moments for 15R-BaFeO$_2$F and 15R-BaFeO$_{2.25}$F$_{0.5}$ align in the a/b-plane with antiferromagnetic alignment of the moments between adjacent layers, and are flipped by 90° as compared to the precursor compound. 15R-BaFeO$_2$F exhibits very robust antiferromagnetism with a Néel temperature between 300 and 400 °C.

1. Introduction

Iron-containing perovskite compounds of the type A$^{[12]}$B$^{[6]}$X$_3$ (B=Fe and other transition metals) show a wide range of applications such as fuel cell cathodes, gas separation membranes and sensors [1–3]. Among them, the BaFeX$_{3-d}$ compounds show interesting magnetic properties ranging from ferromagnetic- to antiferromagnetic-alignment of the magnetic moments [4–7].

Perovskite structures are usually described in terms of the B cations occupying 1/4 of the octahedral sites in a close packed arrangement of AX$_3$ layers [8]. If a layer A is surrounded by two layers with different orientation (e.g. B A C), it is assigned the letter c in the Jagodzinski notation [8]; if the layer A is surrounded by two layers with the same orientation (e.g. B A B), it is assigned the letter h in the Jagodzinski notation [8]. For a stapling sequence ccc…, the simple cubic perovskite structure (as found for example in SrFeO$_3$ [9]) is formed, whereas the hexagonal perovskite structure is obtained for the sequence hhh… (for example in BaCoO$_3$ [10]). A huge variety of stapling sequences between those boundaries are also known, e.g. cch.. for 6H-BaFeO$_{3-d}$ [11–14], cchch… for 15R-BaFeO$_{3-d}$F$_y$ [15,16] and cchh… for 12R-BaFeO$_{3-d}$ [4,14]. The nature of the connectivity of the iron octahedra via faces or corners depends on the type of surrounding layers. The connexion to iron atoms via a c-type layer is only by corners, whereas face sharing is found if the iron atoms are connected by a h-type layer.

The kind of perovskite-type structure formed can be related to the Goldschmidt's tolerance factor [17], which is a simple geometric expression calculated from the ionic radii of the A, B and X ions and is based on the ratio of the lengths of the edge- and the face-diagonal of the primitive cubic perovskite structure. Hence, the type of structure formed can be influenced by changing the size of the transition metal cation by, for example, a change in oxidation state. For BaFeO$_{3-d}$ this can be done by tuning the synthesis conditions and a variety of BaFeO$_{3-d}$ compounds (with different values of d) can be made by applying different oxygen partial pressures and reaction temperatures, e.g. BaFeO$_{2.5}$ (P2$_1$/c, vacancy ordered variant of the cubic perovskite) [11,18] from preparation under N$_2$; 6H-BaFeO$_{-2.8}$ (P6$_3$/mmc) from heating under 1 bar oxygen atmosphere [14]; and 12R-BaFeO$_{-2.9}$ (R3m) from heating at elevated oxygen partial pressures (> 5 bar) [14].

At lower temperatures, the Ba/Fe sublattice is relatively stable and this, combined with good anion mobility, can be used to modify the anion sublattice/ iron oxidation state. For example, Hayashi et al. [5] showed that cubic, ferromagnetic BaFeO$_3$ can be made by heating BaFeO$_{2.5}$ at 200 °C under an O$_3$ atmosphere. Therefore, low temperature modification methods [19] can be used to modify a preformed perovskite sublattice.

In general, high levels of anion vacancies favour the formation of structures related to the cubic perovskite [20]. Recently, Sturza

* Corresponding author. Fax: +44 121 4144403.
E-mail address: oliverclemens@online.de (O. Clemens).

et al. showed that the addition of fluoride ions into the starting mixtures in high temperature synthesis routes contributes to the anion lattice remaining filled by lowering the average oxidation state of the Fe cation. In this way 15R-BaFeO$_{3-d}$F$_y$ (0.15≤y≤0.30) was prepared [15,16,21] with average iron oxidation states close to +III.

In contrast, high amounts of fluoride ions cannot usually be stabilised in alkaline earth-containing oxide compounds at high temperatures [22]. This is related to the high stability of the alkaline earth (AE) fluorides AEF$_2$. A variety of fluorination agents can be used to modify the anion sublattice and the oxidation state of the transition metal in a preformed oxide, for example CuF$_2$ [23], F$_2$ [24] and XeF$_2$ [25] have all been used for this purpose. In 2002, polyvinylidenedifluoride (PVDF) was shown to be a useful fluorination agent [22] and can be used for the synthesis of a variety of iron-containing oxide fluoride perovskite compounds with a high fluorine content, e.g. cubic BaFeO$_2$F [26,27], SrFeO$_2$F [28,29], Sr$_x$Ba$_{1-x}$FeO$_2$F [30,31], La$_{1-x}$SrFeO$_3$$_{-x}F_x$ [32,33] and hexagonal 6H-BaFeO$_2$F [34]. The high stability of the Ba/Fe sublattice and nature of PVDF as a low temperature fluorination agent allows the synthesis of different modifications of the metastable compound BaFeO$_2$F. Recently, Anji Reddy and Fichtner [35] showed that the fabrication of a fluoride ion battery is, in principle, possible and this opens up possible applications of oxide fluoride compounds as electrode materials for this application [36].

Cubic- and hexagonal-(6H) BaFeO$_2$F show highly robust antiferromagnetic ordering (T$_N$~600–700 K) [27,34]. For both compounds, the presence of iron as Fe^{3+} helps stabilise the magnetic ordering temperature (e.g. 6H-BaFeO$_{3-d}$ has an ordering temperature below 200 K [13]). In addition, cubic BaFeO$_2$F shows G-type ordering of the magnetic moments [27], whereas the moments of the Fe^{3+} ions in 6H-BaFeO$_2$F order antiferromagnetically between adjacent layers along the c-axis [34].

In this article we report the first synthesis of the compounds 15R-BaFeO$_2$F and 15R-BaFeO$_{3-d}$F$_{0.5}$ by low temperature fluorination of 15R-BaFeO$_{3-d}$F$_{0.2}$ using PVDF as a fluorination agent. The crystal and magnetic structures of both compounds have been examined by X-ray- and neutron-powder diffraction studies. Bond valence sums (BVS) have been used to elucidate the distribution of the oxide/fluoride ions and these suggest anion ordering in 15R-BaFeO$_2$F. This insight has provoked us to apply BVS to our recently published structure of 6H-BaFeO$_2$F [34] in greater detail, and we report here on an ordering between the oxide and fluoride ions in this compound and a revised structure.

2. Experimental

2.1. Sample preparation

The precursor oxide fluoride 15R-BaFeO$_{3-d}$F$_{0.2}$ was prepared by a solid state reaction between stoichiometric mixtures of high purity BaF$_2$, BaCO$_3$ and Fe$_2$O$_3$ powders (Sigma Aldrich,≤99.9%) which were ground using a planetary ball mill (Fritsch pulverisette 7, 350 rpm, 1.33 h), pressed to pellets to minimise the contact area to the surrounding atmosphere, and heated at 900 °C for 12 h under air in a covered alumina crucible. The samples were quenched to room temperature.

The oxide fluorides of composition 15R-BaFeO$_{3-d}$F$_y$ (y=0.5, 1) were prepared from stoichiometric amounts of the as prepared 15R-BaFeO$_{3-d}$F$_{0.2}$ and polyvinylidenedifluoride (PVDF), which were thoroughly ground in n-pentane (for the synthesis of 15R-BaFeO$_2$F, y=1, a 4% excess of PVDF was used). The mixtures were slowly heated to 370 °C (20 °C/h) under air and kept at this temperature for 20 h; slow heating was found to be beneficial to synthesise a product free of BaF$_2$ impurities.

Structural studies were focused on the 15R-BaFeO$_2$F phase, which was shown to be metastable and its thermal decomposition was confirmed by examining the decomposition products arising from heating at 900 °C for 5 min in air.

2.2. Diffraction experiments

X-ray diffraction (XRD) patterns were recorded on a Bruker D8 diffractometer with Bragg–Brentano geometry and a fine focus X-ray tube with Cu anode. A primary beam monochromator was attached. A LYNXEYE detector and fixed divergence slit were used. The total scan time was 16 h for the angular range between 5° and 140° 2θ.

Time of flight powder neutron diffraction (NPD) data were recorded on the HRPD high resolution diffractometer at the ISIS pulsed spallation source (Rutherford Appleton Laboratory, UK). 4 g of powdered 15R-BaFeO$_{3-d}$F$_{0.5}$ and 15R-BaFeO$_2$F were loaded into 8 mm diameter thin-walled cylindrical vanadium sample cans. Data were collected at ambient temperature for 75 μAh proton beam current to the ISIS target (corresponding to ~2 h beamtime) for each sample. 15R-BaFeO$_2$F was also investigated at 300 °C and 400 °C to estimate the Néel temperature.

Structure refinements using both the XRD and NPD data were performed using the Rietveld method [37,38] with the programme TOPAS 4.2 (Bruker AXS, Karlsruhe, Germany) [39]. For the room temperature XRD data the whole 2θ-range was used, while for the NPD data only those data collected in the highest resolution backscattering detector bank (bank 1, average 2θ=168.329°, d$_{max}$~2.5 Å) were used. The instrumental intensity distribution for the X-ray data was determined empirically from a sort of fundamental parameters set [40] using a reference scan of LaB$_6$. The microstructural parameters were refined to adjust the peak shapes for the XRD data. For the neutron diffraction data, a corresponding TOF shape model was used. Lattice parameters were constrained to be the same for neutron- and XRD-data and the same positional parameters were used and refined for both data sets. Independent thermal displacement parameters were refined for each type of atom, but these for O and F on the same site were constrained to the same value (for the O1/F1 site in 15R-BaFeO$_2$F). While these parameters were also constrained to be the same both for X-ray- and neutron-powder diffraction data, an additional B overall value was refined for XRD data accounting for further effects such as absorption or surface roughness. Reflections that showed a large magnetic scattering contribution were omitted from the initial crystallographic refinement. For 15R-BaFeO$_{2.25}$F$_{0.5}$, the thermal parameters of the Ba ions and O/F ions were constrained to be the same to allow for refinement of the site occupancies.

Refinements of the magnetic structures of 15R-BaFeO$_2$F and 15R-BaFeO$_{3-d}$F$_{0.5}$ were performed with the programme GSAS [41,42] using the NPD data collected in all of the HRPD detector banks. The magnetic contribution to the diffraction pattern was modelled by introducing a second phase in triclinic space group P1 with a doubled length (therefore containing twice the number of atoms) of the trigonal c-axis containing just Fe atoms (to allow for an easier determination of the orientation of the magnetic moments) and calculating only its magnetic scattering. Unit cell, atomic positions and thermal vibration parameters in this second phase were set to the refined values determined above and then fixed to ensure that the triclinic (P1) cell remained geometrically and symmetrically equivalent to the R-3m cell doubled along the c-axis. Different orientations of the magnetic moments were investigated, including those previously reported for similar compounds [16].

2.3. Magnetic measurements

DC susceptibility measurements were performed over the temperature range 5–300 K using a Quantum Design MPMS SQUID magnetometer. The samples were pre-cooled to 5 K in zero field (ZFC) and also in an applied field of 0.05 T (FC) and values of χ measured whilst warming in a field of 0.05 T. Field-dependent DC

susceptibility measurements were performed on the same instrument at 5 K between 0 and 5 T.

2.4. Mössbauer measurements

The ^{57}Fe Mössbauer spectrum for 15R-BaFeO$_2$F was recorded in constant acceleration mode using a ca. 25 mCi ^{57}Co/Rh source at 300 K.

2.5. Quantum mechanical calculations

Quantum mechanical calculations were performed to calculate the structure of anion ordered 6H-BaFeO$_2$F and 6H-BaFeO$_3$ using a density functional approach with GGA, as implemented in the programme Castep [43]. The calculations were based on the use of ultrasoft pseudopotentials and of plane waves as basis functions. The cutoff energy of the latter was set equal to 300 eV. As the criterion for convergence we required that the total energy converged to 0.00002 eV per atom, a maximum stress of 0.1 GPa and that the forces acting on the atoms were smaller than 0.05 eV/Å. The functional of Perdew, Burke and Ernzerhof (PBE) [44] was used to describe the effects of exchange and correlation. A k-grid of $4 \times 4 \times 2$ was used without further optimisation of the number of k points.

3. Results and discussion

3.1. The crystal structure of 6H-BaFeO$_2$F—a reinvestigation

We recently [34] discussed the possibility of oxide and fluoride being randomly distributed on the two anion sites in the compound 6H-BaFeO$_2$F, but occupying slightly different positions. Such a split site model [34] used two slightly different sites for the oxygen and fluoride ions with occupancies of 2/3 and 1/3. In the context of our investigations of 15R-BaFeO$_2$F described in Section 3.2 we think that at least a partially (if not fully) ordered distribution of the oxide and fluoride ions is more likely in this compound and that the fluoride ions form a h-type layer of composition BaF$_3$ between the Fe^{3+} cations which show a face sharing of the octahedra. We account for this assumption as follows:

– The off-centre shift of the iron cations in the face sharing octahedra is remarkably high. At first, we assumed that this was due to a high degree of cation repulsion between these relatively close cations. We therefore compared the crystal structures of similar compounds reported in literature and found that whereas the difference between the iron–anion distances in the face sharing layers and those in the corner sharing layers is remarkably high (Δ~0.27 Å) for 6H-BaFeO$_2$F, it is much lower in 6H-BaTiO$_3$ (0.03 Å [45]) and 6H-BaFeO$_{3-d}$ (0.06 Å [4]). If cation repulsion constituted the only source for this off-centre displacement in 6H-BaFeO$_2$F, the distances would be expected to be less different. Furthermore, in the compound 15R-BaFeO$_{2.42}$F$_{0.2}$ [16] which is also reported to show ordering of the fluoride ions into h-type layers, the difference between the Fe–O distances in face sharing octahedra is significantly more pronounced (0.12–0.15 Å [16]).
– These differences in off-centre shift were also confirmed by ab initio structure calculations. We calculated the structures for an ordered 6H-BaFeO$_2$F compound (all the F$^-$ in the h-type layer) as well as the structure for 6H-BaFeO$_3$. For 6H-BaFeO$_2$F the Fe–F and Fe–O distances for Fe on the 4f site were remarkably different (2.22 vs. 1.85 Å), in good agreement with our experimental findings. For 6H-BaFeO$_3$ the distances of the Fe to the h- and c-type layers were far more regular (1.95 vs. 1.90 Å), again in agreement with comparisons with other reported structures.

Table 1
Bond valence sums for different models of oxide/fluoride distribution in 6H-BaFeO$_2$F.

6H-BaFeO$_2$F	Split sites for O^{2-} and F$^-$ with random distribution as reported in [34]	O^{2-} occupying the 12k site, F$^-$ occupying the 6h site
Ba1 (2b)	+2.13	+2.03
Ba2 (4f)	+2.07	+2.11
Fe1 (2a)	+2.66	+2.83
Fe2 (4f)	+2.80	+2.77
O1 (12k)	−1.82	−1.83
F1 (12k)	−1.49	–
O2 (6h)	−1.54	–
F2 (6h)	−1.16	−1.22
Global Instability Index (GII)	0.59 v.u.	0.17 v.u.

– The bond valence sums from both models (see Table 1) are in relatively good agreement for the cations in 6H-BaFeO$_2$F. Nevertheless, the anion charges (which we did not calculate in our previous study [34]) favour the occupancy of the 12k anion site by oxygen and of the 6h site by fluoride. In particular, the bond valences of F in the F1 (12k) site and O in the O2 (6h) sites are high and low respectively in the random distribution model, while more sensible bond valences are found for the ordered model. This is also in agreement with a lower observed Global Instability Index (GII) for the ordered distribution.

Complete ordering of the O^{2-} and F$^-$ ions would require the charges of the (BaO$_3$)$^{4-}$ and (BaF$_3$)$^{1-}$ layers to be very different. Although the oxide- is larger than the fluoride-ion (Δ~0.07 Å [46]) and would be expected to show slightly larger distances as compared to fluoride, the higher negative charge on this layer overcompensates the size effect such that Fe^{3+} suffers a higher attractive force, leading to a reduction in the distance to the (BaO$_3$)$^{4-}$ layers.

Our investigations suggest that ordering of oxide- and fluoride-ions therefore may occur in 6H-BaFeO$_2$F and this proposal is endorsed by our investigations of the 15R type phases reported in Section 3.2. Hence, our previously reported split site model for 6H-BaFeO$_2$F might more reasonably be interpreted in terms of describing the thermal motion of anions. The revised structure of 6H-BaFeO$_2$F is shown in Table 2. It is worth mentioning that differentiation between different anion distributions can only be made by such a posteriori considerations of cation–anion distances, since the goodness of fit values are nearly identical for both models due to the nearly identical scattering powers for both O^{2-} and F$^-$ in XRD and NPD (as described in more detail in [34]). Anisotropic thermal parameters can be used to improve the fit slightly further (with a ΔR_{wp}~0.1) but do not contribute to a better qualitative understanding of the structure.

3.2. Structural characterisation of 15R-BaFeO$_2$F and 15R-BaFeO$_{3-d}$F$_{0.5}$

3.2.1. Structural characterisation of 15R-BaFeO$_2$F

Fluorination of the precursor oxide 15R-BaFeO$_{3-d}$F$_{0.2}$ using a 4 mol% excess of PVDF under air resulted in the formation of a fine brown powder.

The ^{57}Fe Mössbauer spectrum recorded at 298 K was best fitted to three sextets as shown in Fig. 1. The ^{57}Fe Mossbauer parameters are contained in Table 3. The isomer shifts are all characteristic of Fe^{3+}. The relative areas of the sextets reflect the presence of the different iron sites. The presence of magnetically ordered components in the spectrum implies magnetic ordering at room temperature (for further discussion see Section 3.3). Although the

Table 2
Revised structural data for 6H-BaFeO$_2$F (space group $P6_3/mmc$) from a coupled Rietveld analysis of XRD and POLARIS bank 5 NPD data, assuming ordering of the O^{2-} and F$^-$ ions on the 12k and 6h sites.

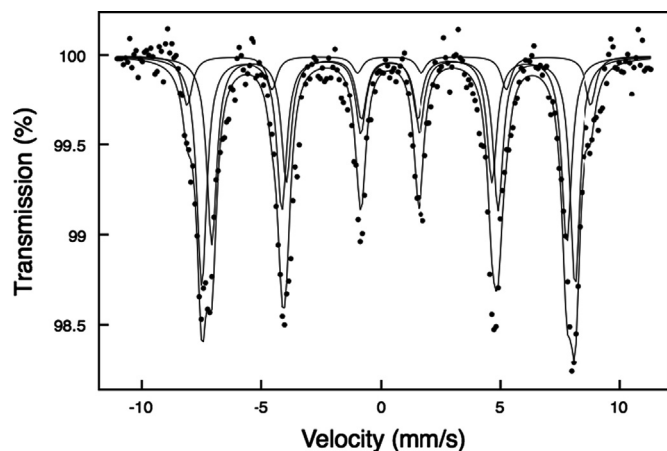| Atom	Wyckoff site	x	y	z	Occupancy	B [Å²]
Ba^{2+}	Ba1/2b	0	0	1/4	1	0.54(3)
Ba^{2+}	Ba2/4f	1/3	2/3	0.08939(6)	1	0.43(2)
Fe^{3+}	Fe1/2a	0	0	0	1	1.50(3)
Fe^{3+}	Fe2/4f	1/3	2/3	0.85257(6)	1	1.16(3)
O^{2-}	O1/12k	0.1661(1)	0.8339(1)	0.5822(1)	1	0.95(1)
F$^-$	F1/6h	0.5094(2)	0.4906(2)	1/4	1	1.29(2)
a [Å]		5.76350(4)	c [Å]	14.2119(1)	V [Å³]	408.842(7)
R_{wp} (XRD+NPD)		2.718	GOF (XRD+NPD)	2.19	R_{Bragg}	0.64 (XRD)
						2.89 (NPD)

Fig. 1. ^{57}Fe Mössbauer spectrum recorded at 298 K from 15R-BaFeO$_2$F. Total fit and partial fits for the 3 different Fe components are shown.

Table 3
^{57}Fe Mössbauer parameters recorded at 298 K from 15R-BaFeO$_2$F.

Temperature (K)	$\Delta \pm 0.02$ (mm/s)	$e^2qQ/2 \pm 0.02$ (mm/s)	$H \pm 0.05$ (T)	Relative area ± 3 (%)
298	0.46	−0.08	52.4	12
	0.33	−0.06	48.4	41
	0.37	−0.02	46.1	47

spectra recorded from cubic BaFeO$_2$F [27] and 6H-BaFeO$_2$F [34] also showed that iron adopts only the Fe^{3+} oxidation state, the details of the magnetic components of the spectra are different in each case. This will be the subject of a further more detailed Mössbauer investigation of all these phases as a function of decreasing temperature and will be the substance of a subsequent report. In combination with the neutron powder diffraction studies (which show a completely filled anion sublattice) the spectrum is consistent with the sample composition of BaFeO$_2$F.

We also report that 15R-BaFeO$_2$F decomposed at elevated temperatures in a fashion similar to that of cubic BaFeO$_2$F and 6H-BaFeO$_2$F [31,34].

$$BaFeO_2F \rightarrow 0.5\ BaFe_2O_4 + 0.5\ BaF_2$$

The decomposition appears to be driven by the high stability of the alkaline earth (AE) fluorides AEF$_2$ as is also known for other highly fluorinated compounds such as SrFeO$_2$F [31], Sr$_2$TiO$_3$F$_2$ and Ca$_2$CuO$_2$F$_2$ [22]. Quantification of the decomposition products by Rietveld analysis confirmed the sample composition of these
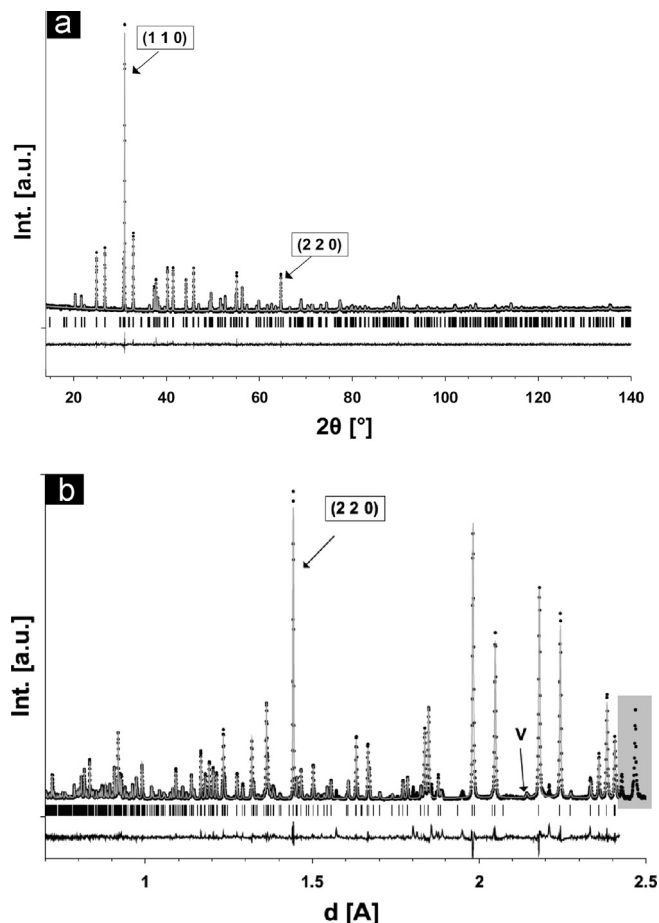

Fig. 2. Coupled Rietveld analysis of XRD (a) and HRPD bank 1 NPD (b) data. Measured data points (black circles), calculated pattern (grey curve), difference curve (black) and Bragg markers for 15R-BaFeO$_2$F are shown. Additional reflections in the NPD pattern are due to magnetic scattering (see Section 3.3.2).

metastable compounds [31,33,34]. After decomposing the 15R-BaFeO$_2$F phase at 900 °C for 5 min, BaFe$_2$O$_4$ ($Cmc2_1$) and BaF$_2$ (Fm-$3m$) were found in quantities of 49.4(2) and 50.6(2) mol%, confirming the reaction equation shown above and providing further support for the composition of the compound as BaFeO$_2$F. A coupled Rietveld analysis of XRD and HRPD bank 1 diffraction data (see Fig. 2) was performed on the compound 15R-BaFeO$_2$F assuming the same space group (R-$3m$) that was found for the precursor compound. The ($h\,k\,0$) reflections show a lower FWHM than the other ($h\,k\,l$) reflections. This might be explained by anisotropy of crystallite size/strain along the c-axis (e.g. caused by stacking faults); other effects such as texture can be eliminated since it was observed in both XRD- and NPD-data (which were

recorded using different geometries; reflection vs. transmission). We therefore allowed for an independent refinement of the peak width for the $(h\,k\,0)$ reflections to allow for a detailed analysis of the structural parameters.

The refined crystal structure is shown in Fig. 3, and the refined structural data are listed in Table 5. The Rietveld analysis showed that the anion sites are fully occupied by O/F ions. Both ions are nearly indistinguishable using XRD/NPD due to essentially indistinguishable scattering lengths, respectively. Similar to 6H-$BaFeO_2F$, the distances of the Fe1/Fe2 ions, which are located in the face sharing octahedra, to the anions linking by face respectively by corner are quite different ($\Delta=0.267(6)$ Å for Fe1 and $\Delta=0.252(4)$ Å for Fe2). This difference cannot be explained by pure cation repulsion due to face sharing (as already discussed for 6H-$BaFeO_2F$ in Section 3.1) and is even larger as compared to the parent compound. As above, bond valence sums suggest an ordering of the oxide and fluoride ions on the different anion sites (see Table 4). In contrast to 6H-$BaFeO_2F$, the anion site that connects the Fe1 and Fe2 octahedra by faces must have a partial occupation by O^{2-} of 1/6 due to the composition of the compound.
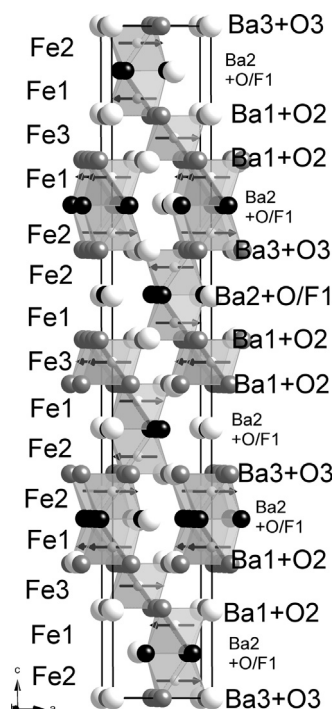
This is consistent with the relatively high thermal parameter of the site, which might indicate reduced ordering on that position.

The higher thermal parameter of the O1/F1 site can also be attributed to the smaller size of the fluoride ions. Since oxide is the larger anion, the BaO_3 layers show a much higher expansion than the $Ba(O_{1/6}F_{5/6})_3$ layers and dominate the expansion in the a/b-plane. Hence, we suggest that the F^- ions have more space to vibrate in this otherwise close packed h-layer. Furthermore, 15R-$BaFeO_{2.27}F_{0.5}$ (see Section 3.2.2) shows a high degree of disorder in the hexagonal layers which possess vacancies, oxide- and fluoride-ions and requires the occupation of an additional anion site to appropriately describe the structure. No evidence for the occupancy of such a site is found in the fully fluorinated 15R-$BaFeO_2F$, and a fully occupied close packed BaX_3 layer is sterically prohibitive to the occupancy of such an additional site.

3.2.2. Structural characterisation of 15R-$BaFeO_{3-d}F_{0.5}$

Partial fluorination of the compound 15R-$BaFeO_{3-d}F_{0.2}$ using PVDF was achieved by adapting the amount of the polymer to the desired degree of fluorination. Therefore, it proved possible to prepare compounds with composition 15R-$BaFeO_{3-d}F_y$ ($0.2 \le y \le 1$) using this method. This was also observed for 6H-$BaFeO_{3-d}F_y$ [34], where adjustment of the fluorine content is possible for $0 < y \le 1$. However, this does not apply to all perovskite-related compounds since a hypothetical phase $SrFeO_{2.5}F_{0.5}$ was recently shown to decompose into $SrFeO_3$ and $SrFeO_2F$ [47].

15R-$BaFeO_{3-d}F_{0.5}$ was obtained as a black powder and investigated by a coupled Rietveld analysis of X-ray- and neutron-powder diffraction data (see Table 6 for the refined structure). As was shown by Mössbauer studies reported by Sturza et al. [16] and by a detailed analysis of lattice parameters for the 6H-$BaFeO_{3-d}F_y$

Fig. 3. Crystallographic and (excerpt of the) magnetic structure of 15R-$BaFeO_2F$. The F1/O1 anion site (black ions) is occupied by 83.33% of F^- and 16.67% of O^{2-}.

Table 5
Bond valence sums for different models of oxide/fluoride distributions in 15R-$BaFeO_2F$.

15R-$BaFeO_2F$	Random disorder of oxide and fluoride ions	Ordering of oxide and fluoride ions
Ba1	2.08	2.14
Ba2	2.11	2.06
Ba3	1.97	1.95
Fe1	2.77	2.79
Fe2	2.75	2.76
Fe3	2.66	2.80
O1	1.42 (66.67%)	1.41 (16.67%)
F1	1.15 (33.33%)	1.15 (83.33%)
O2	1.85 (66.67%)	1.85
F2	1.52 (33.33%)	–
O3	1.99 (66.67%)	1.99
F3	1.52 (33.33%)	–

Table 4
Structural data for 15R-$BaFeO_2F$ (space group $R\text{-}3m$) from a coupled Rietveld analysis of XRD and HRPD bank 1 NPD data.

Atom	Wyckoff site	x	y	z	Occupancy	B [Å²]
Ba^{2+}	Ba1/6c	0	0	0.13099(5)	1	0.40(4)
Ba^{2+}	Ba2/6c	0	0	0.40174(4)	1	0.29(4)
Ba^{2+}	Ba3/3a	0	0	0	1	0.48(5)
Fe^{3+}	Fe1/6c	0	0	0.22494(4)	1	1.20(3)
Fe^{3+}	Fe2/6c	0	0	0.30779(4)	1	0.38(3)
Fe^{3+}	Fe3/3b	0	0	$^1/_2$	1	1.15(4)
O^{2-}	O1/18h	0.4919(2)	0.5081(2)	0.39996(4)	1/6	1.50(4)
F^-	F1/18h				5/6	1.50(4)
O^{2-}	O2/18h	0.4992(2)	0.5008(2)	0.13364(4)	1	0.74(4)
O^{2-}	O3/9e	1/2	0	0	1	0.51(4)
a [Å]	5.7659(1)	**c [Å]**		35.7149(9)	**V [Å³]**	1028.271(58)
R_{wp} (XRD+NPD)	3.72	**GOF (XRD+NPD)**		2.97	**R_{Bragg}**	2.04 (XRD) 1.73 (NPD)

Table 6
Structural data for 15R-$BaFeO_{2.25}F_{0.5}$ (refined composition $BaFe(O/F)_{2.73}$; space group $R\text{-}3m$) from a coupled Rietveld analysis of XRD and HRPD bank 1 NPD data.

Atom	Wyckoff site	x	y	z	Occupancy	B [Å²]
Ba^{2+}	Ba1/6c	0	0	0.13180(6)	1	0.54(3)
Ba^{2+}	Ba2/6c	0	0	0.40275(6)	1	0.54(3)
Ba^{2+}	Ba3'/6c	0	0	0.0074(11)	0.5	0.54(3)
Fe^{3+}	Fe1/6c	0	0	0.22423(6)	1	1.11(5)
Fe^{3+}	Fe2/6c	0	0	0.30791(6)	1	0.69(4)
Fe^{3+}	Fe3/3b	0	0	1/2	1	0.65(5)
O^{2-}/F^{-1}	O1a/18h	0.4758(5)	0.5242(5)	0.4022(2)	0.526(10)	0.99(2)
O^{2-}/F^{-1}	O1b/18h	0.518(2)	0.482(2)	0.3919(5)	0.158(10)	0.99(2)
O^{2-}/F^{-1}	O1c/18h	0.599(2)	0.401(2)	0.3957(6)	0.087(5)	0.99(2)
O^{2-}	O2/18h	0.5000(2)	0.5000(2)	0.13350(5)	1	0.99(2)
O^{2-}	O3/9e	1/2	0	0	1	0.99(2)
a [Å]	5.7489(2)	c [Å]	35.894(1)	V [Å³]	1027.35(6)	
R_{wp} (XRD+NPD)	5.08	GOF (XRD+NPD)	4.07	R_{Bragg}	2.53 (XRD) 3.60 (NPD)	

compounds [34], such partially fluorinated phases can contain traces of Fe^{4+}. The refinement allowed for the determination of an approximate sample composition of $BaFe(O/F)_{2.73}$, indicating that the sample contains mainly Fe^{3+} (a further decrease in lattice parameters was observed when heating the sample in O_2, indicating the possibility of further oxidation). The real anion content is likely to be slightly higher, but occupancies and thermal parameters are known to be strongly correlated for such refinements, which makes it nearly impossible to determine an exact oxygen composition within 1–2% of error. However, the presence of Fe^{2+} can be ruled out from the preparation conditions and has never been observed in such oxide fluoride compounds. We therefore assume the composition to be close to $BaFeO_{2.25}F_{0.5}$, which would be the correct formula assuming full incorporation of F^- and Fe^{3+} only. 15R-$BaFeO_{2.25}F_{0.5}$ also decomposed at elevated temperatures into BaF_2 (12.0 mol%), $BaFe_2O_4$ (13.1 mol%) and another 15R-$BaFeO_{3-d}F_y$ phase (~74.9 mol%), for which y can be assumed to be 0.35 [15] (15R-$BaFeO_{3-d}F_{0.35}$ was reported to be the highest F content phase that could be prepared by high temperature reaction [15]). The overall composition after decomposition was therefore determined to be $Ba_1Fe_{1.01}O_{2.25}F_{0.50}$, and the fluorine content is again in excellent agreement with that expected from the amount of PVDF used for the fluorination. This composition is also in agreement with the composition of $BaFe(O/F)_{2.73}$ from the Rietveld analysis (see Table 6).

Furthermore, the Rietveld analysis showed the vacancies to be mainly located in the hexagonal layers. As was already observed for 15R-$BaFeO_{2.42}F_{0.2}$ by Sturza et al. [15] the anions in the hexagonal layers (O1a–c ions) are much less localised than those in the cubic layers (O2+3 ions). Hence, the anions are spread onto the position O1c, which was not found to be occupied if the layer is completely filled by anions, i. e. the refinement of this position did not prove to be stable for 15R-$BaFeO_2F$. Therefore only a single O1 site (most similar to O1a) was used for 15R-$BaFeO_2F$. Due to the increased filling of the sublattice compared to the precursor 15R-$BaFeO_{2.42}F_{0.2}$ [16], the O1a+b sites show a higher occupancy than in the precursor compound (Δ~0.1 for each site), whereas the occupancy of the O1c site remains roughly the same. In addition, the O1a and O1b sites (see Fig. 4a) shift towards the ideal O1 site found for 15R-$BaFeO_2F$ (Fig. 4c) compared to the precursor 15R-$BaFeO_{2.42}F_{0.2}$ (Fig. 4b). Also, the O1c site shows a much lower degree of deviation from the more ideal O1a/O1b sites found for 15R-$BaFeO_{2.42}F_{0.2}$ [16] and the distance between O1a and O1b is much shorter for 15R-$BaFeO_{2.25}F_{0.5}$ (by about 0.30 Å) indicating a higher localisation of the anions on the ideal sites for a close packing model, as well as an increased filling of the h-type layers for the higher fluorinated compound. Nevertheless, the split position is still necessary for a good description of the reflection
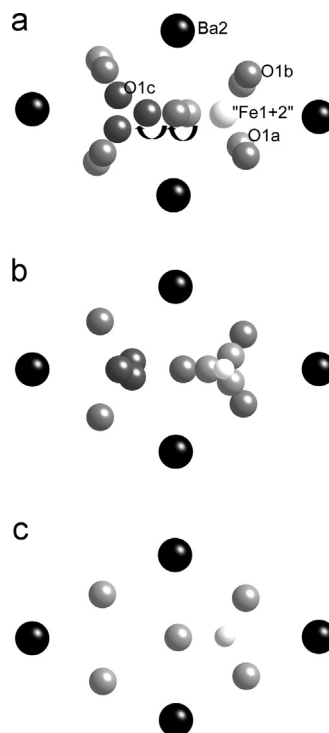

Fig. 4. (a) Distribution of the anions in the hexagonal layers in the compound 15R-$BaFeO_{2.25}F_{0.5}$. Fe1/Fe2 are located above and below the layer. Ba3' is located above and below the triangle formed of the O1c ions. (b) Distribution of the anions in the hexagonal layers in the compound 15R-$BaFeO_{2.42}F_{0.2}$ as reported by Sturza et al. [15]. (c) Distribution of the anions in the hexagonal layers in the compound 15R-$BaFeO_2F$.

intensity and improves the fit significantly. The low localisation of the anions in the hexagonal layers was shown to promote oxygen mobility for 15R-$BaFeO_{2.42}F_{0.2}$ [16] and this might also be the case in the higher fluorinated compounds, although the mobility would be expected to be lower due to the increased filling of the h-type layer. The possible conduction pathway is indicated with arrows in Fig. 4a.

Bond valence sums again indicate that the fluoride ions should be preferably located in the hexagonal layers (assuming oxygen on O1a–c: 1.39, 1.56, 1.71; O2: 1.91; O3: 2.01). The composition of the hexagonal layer would be $BaF_{10/24}O_{9/24}F_{5/24}$ assuming a formula of $BaFeO_{2.25}F_{0.5}$ and full incorporation of the F^- ions into the h-type layer. Vacancies in the h-layers were reported to cause square pyramidal and even tetrahedral coordination for 15R-$BaFeO_{2.42}F_{0.2}$ (h-layer composition ~$BaF_{1/6}O_{1/2}F_{1/3}$). Since ~1/5 of the anion sites in the hexagonal layers are empty for 15R-$BaFeO_{2.25}F_{0.5}$, at least every second coordination polyhedron of the Fe1/Fe2 ions would

be required to have a coordination number of 5. This also means that the overall coordination number of the Fe1/Fe2 must increase compared to the precursor compound. This is also expressed by the change of the position of the oxygen ions compared to the precursor (see Fig. 4b). For 15R-$BaFeO_{2.42}F_{0.2}$, the oxygen ions move more towards the 1/3 2/3 z position in the hexagonal layer, which is just above the Fe atoms. In addition, the site above the Ba cation is also occupied to higher degree as in 15R-$BaFeO_{2.25}F_{0.5}$, which is in agreement with the different amount of vacancies in the layer. For 15R-$BaFeO_2F$ (see Fig. 4c), the layer is dense packed and the O1c position cannot be occupied for space reasons. The partial occupancy of the O1c site in the 15-$BaFeO_{2.25}F_{0.5}$ is also indicated by a high displacement of the Ba3' site; Ba3' moves towards the O1c ion due to its Coulomb attraction. In contrast, a much higher localisation of the Ba3 atom is observed for 15R-$BaFeO_2F$ (if one assumes a Ba3' atom, it remains much closer to the ideal Wyckoff position 3a and therefore the ideal Wyckoff site 3a was used for the refinement of 15R-$BaFeO_2F$; d(Ba3'–Ba3')=0.14 Å in $BaFeO_2F$ vs. 0.53 Å for 15R-$BaFeO_{2.25}F_{0.5}$).

The distribution of the ions in the low fluorine-containing compounds also gives an insight into the mechanism of the fluorination reaction. Since vacancies are preferably located in the hexagonal layers, the ionic conductivity in the hexagonal layers is probably much higher than in the cubic layers, which is also suggested by Sturza et al. [15]. The fluorination at low temperatures is therefore likely to favour the incorporation of the ions into the hexagonal layers to enable their easier rearrangement.

3.3. Magnetic characterisation of 15R-$BaFeO_2F$

3.3.1. SQUID measurements

The compound 15R-$BaFeO_2F$ was characterised by two kinds of measurements: Field Cooled/Zero Field Cooled measurements (FC-ZFC) in a temperature range between 5 and 300 K (see Fig. 5), and a Field Sweep measurement at 5 K (see Fig. 6).

A divergence in the susceptibility between FC and ZFC measurements is clearly observed over the whole temperature range. This is indicative of a weak ferromagnetic component and the measurement is similar to those of 6H-$BaFeO_2F$ [34] and cubic $BaFeO_2F$ [27]. Furthermore, the very small magnitude of the magnetic susceptibility over the whole temperature range indicates that the overall ordering of the magnetic moments is antiferromagnetic.

This weak ferromagnetic moment was also observed in field sweep measurement and the remanent magnetisation can be estimated to be around 0.0012 μ_B and is, again, of similar
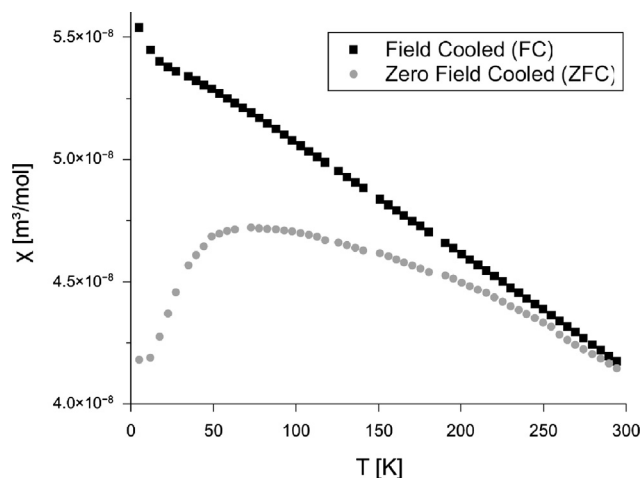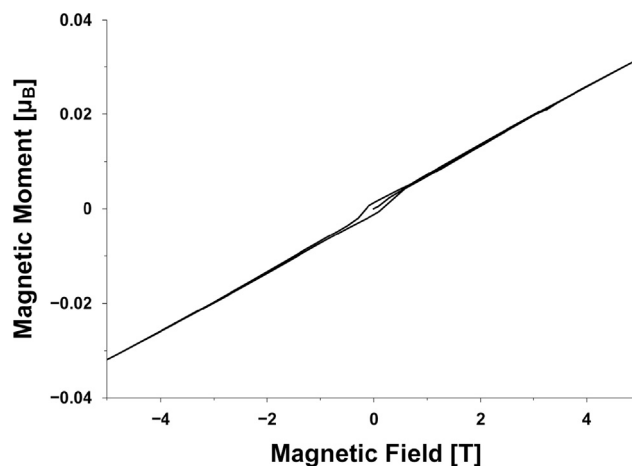

Fig. 6. Field dependent magnetisation per formula unit 15R-$BaFeO_2F$ recorded at 5 K.

magnitude to that found in 6H-$BaFeO_2F$ (0.0025 μ_B [27]) and cubic $BaFeO_2F$ (0.01 μ_B [27]). The remanent magnetisation may be explained by a very small canting angle of the magnetic moments on the iron atoms, which would be out of the detection limit of the neutron powder diffraction measurements (see Section 3.3.2). Furthermore it is interesting to note that the remanent magnetisation appears to decrease in the order cubic to 6H to 15R, whereas the amount of hexagonal stacking sequences increases in the same sequence. In addition, the remanent magnetisation is smaller by about one order of magnitude when compared with the precursor compound 15R-$BaFeO_{3-d}F_{0.2}$ (0.03 μ_B [16]).

3.3.2. Determination of the magnetic structure of 15R-$BaFeO_2F$ and 15R-$BaFeO_{3-d}F_{0.5}$

The neutron diffraction patterns at 298 K showed a strong contribution from magnetic scattering. The additional reflections could be indexed in a trigonal cell with a doubling of the c-axis of the nuclear unit cell (magnetic propagation vector k=(0, 0, 3/2)) and the size of the magnetic unit cell is therefore identical to that of 15R-$BaFeO_{2.42}F_{0.2}$ [16].

Antiferromagnetic alignment of the magnetic moments was evident from the magnetic measurements presented in Section 3.3.1. Along the stacking direction of the Ba(O/F)$_3$-layers, antiferromagnetic alignment of the magnetic moments on the Fe ions between adjacent layers was found for 6H-$BaFeO_2F$ [34], 6H-$Ba_{0.8}Sr_{0.2}FeO_{3-d}F_y$ [16] and 15R-$BaFeO_{3-d}F_y$ [16] and is also the inter-layer order observed for 15R-$BaFeO_2F$.

Two models were tested to determine the alignment of the magnetic moments: parallel to the c-axis (as found for 15R-$BaFeO_{3-d}F_y$ [16] and 6H-$BaFe_{0.67}W_{0.33}O_3$ [48]) and in the ab-plane (as found for 6H-$BaFeO_2F$ [34] and 15R-$BaFe_{0.7}Ir_{0.3}O_{2.949}$ [49]). A reasonable fit was only obtained if the magnetic moments were aligned in the ab-plane (since the exact direction in the a/b-plane cannot be determined using powder diffraction methods [50], an arbitrary alignment along the [1 1 0] direction was chosen; see Fig. 7a and c). Alignment along the c-direction did not give a satisfactory description of the magnetic intensities (Fig. 7b and d).

The magnetic structure is shown in Fig. 3. The magnetic moments on the Fe1, Fe2 and Fe3 ions were determined to be 3.55(3), 3.47(3) and 3.97(4) μ_B and a clear difference of ~0.5 μ_B is therefore obtained for octahedral coordination which involves face and corner sharing (Fe1 and Fe2) as compared to octahedral coordination which involves corner sharing only (Fe3). A similar difference was observed for 6H-$BaFeO_2F$ where the iron atoms which are located in face sharing octahedra show a lower magnetic moment (3.32(3) μ_B) compared to the iron atoms which

Fig. 5. Variation of susceptibility χ of 15R-$BaFeO_2F$ between 5 and 300 K. The data were recorded at increasing temperature in a measuring field of 0.05 T. Separate plots show field cooled (FC) and zero field cooled (ZFC) data.
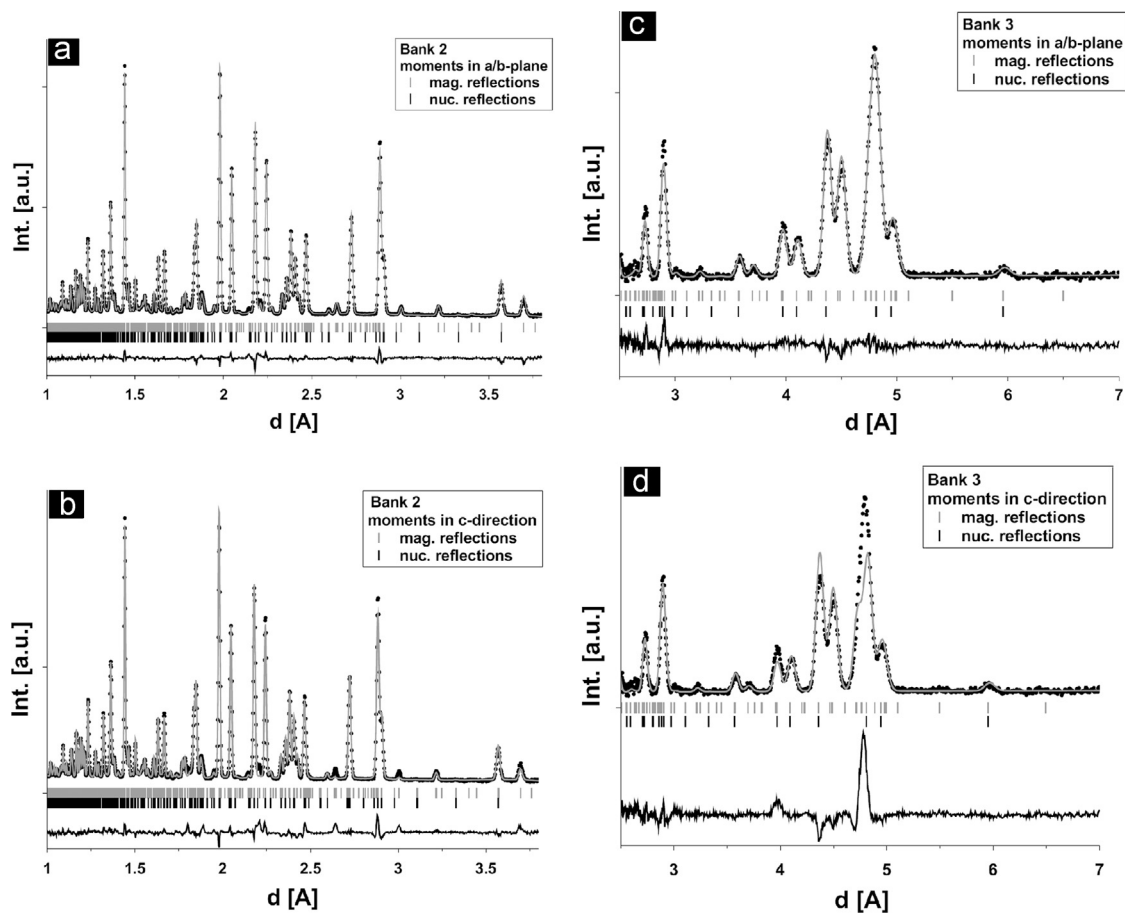
Fig. 7. Refinements of the magnetic structure of 15R-BaFeO$_2$F. Alignment of the magnetic moments in the a/b-plane (bank 2 (a), bank 3 (c)) and along the c-direction (bank 2 (b), bank 3 (d)).

are located in octahedra only connected by corners (3.65(4) μ_B) [34]. The magnetic moment for neutron diffraction is given as $\mu = \mu$spin$+\mu$orbit$-\mu$covalent, and these results indicate that the magnetic moment in the face sharing octahedra is lowered by covalent bonding. This should be expected given the small d–d-overlap of the iron atoms in the face sharing octahedra (see Fig. 3), supported by a relatively short Fe–Fe distance in both compounds; ~2.96 Å for 15R-BaFeO$_2$F and 2.91 Å for 6H-BaFeO$_2$F [34].

The bond angles of Fe1–O2–Fe3 and Fe2–O3–Fe2 are 173.0(1)° and 180.0(0)° (corner shared octahedra), and therefore favour the antiferromagnetic alignment of the magnetic moments between those atoms according to the Goodenough, Kanamori, Anderson (GKA) rules [51]. The Fe1–F1/O1-Fe2 bond angle of 86.4(1)° is close to 90° and would therefore favour ferromagnetic alignment of the moments between those sites. Since the Fe1–Fe2 distance (2.956 (3) Å) is relatively short, direct interactions between the iron atoms can occur. Such interactions can explain the antiferromagnetic alignment of the moments for Fe^{3+} in the d^5 high spin state. This direct interaction is also manifested by the lower magnetic moment of the iron atoms on the Fe1/Fe2 sites and the situation is therefore similar to that in 6H-BaFeO$_2$F [34].

The magnetic ordering breaks down at temperatures between 300 and 400 °C. At 300 °C, we continued to observe magnetic moments on the Fe1–Fe3 atoms with magnitudes of 2.41(8), 1.47 (6) and 3.47(11) μ_B. It is interesting to note that the magnetic moment on the iron atoms in the face sharing octahedra seems to decrease faster than the moment on the iron atom in the corner sharing octahedron. At 400 °C the magnetic reflections completely disappeared. The compound therefore shows very robust antiferromagnetic ordering and its Néel temperature is of a similar

magnitude to that determined for similar compounds such as 15R-BaFeO$_{3-d}$F$_y$ [16], 6H-BaFeO$_{3-d}$F$_y$ [16] and SrFeO$_{2.5}$ [52].

It is very interesting that the alignment of the magnetic moments is flipped by 90° compared to its precursor compound 15R-BaFeO$_{3-d}$F$_{0.2}$ [16]. It is difficult to determine the reason for this change in orientation, but possible explanations might be associated with the lowering of the oxidation state to single valent Fe^{3+} and/or the change in coordination for the iron atoms on the Fe1 and Fe2 site, since partial tetrahedral/square pyramidal coordination has been reported for 15R-BaFeO$_{3-d}$F$_{0.2}$ [16]. A literature search of similar compounds showed that 15R-BaFe$_{0.7}$Ir$_{0.3}$O$_{3-d}$ [49] contains iron in an oxidation state between +3 and +4 and shows an alignment of the magnetic moments in the a/b-plane, whereas the compound 6H-BaFe$_{0.67}$W$_{0.33}$O$_3$ [48] contains only Fe^{3+} and shows alignment of the magnetic moments parallel to c.

An additional investigation of the magnetic structure of the partially fluorinated compound 15R-BaFeO$_{2.25}$F$_{0.5}$ also showed alignment of the magnetic moments in the a/b-plane although the compound contains only little if any traces of Fe^{4+}. This indicates that the increased filling of the anion sites, and therefore change in coordination, might have a dominating influence on the orientation of the moments. The magnetic moments on Fe1–3 were refined to 2.55(4), 3.29(5) and 3.34(6) μ_B.

4. Conclusions

We show here that the compounds 15R-BaFeO$_2$F and 15R-BaFeO$_{2.27}$F$_{0.5}$ can be easily prepared by a low temperature fluorination route using PVDF, hence isolating a third modification of

metastable $BaFeO_2F$. Both compounds show strong evidence of ordering of the oxide and fluoride ions, where the latter preferentially occupies the sites within the hexagonal layers. The composition of the fully fluorinated compound was determined from the quantitative decomposition at elevated temperatures into BaF_2 and $BaFe_2O_4$. This was confirmed by Mössbauer spectroscopy, which showed that iron is present as single valent Fe^{3+}, and, in combination with a completely filled anion sublattice, this is consistent with the formulation $BaFeO_2F$. Furthermore, a reinvestigation of the crystal structure of $6H-BaFeO_2F$ suggested that ordering of oxide and fluoride ions probably takes place in a similar fashion to that observed for $15R-BaFeO_2F$.

The increased filling of the anion sites compared to the precursor compound $15R-BaFeO_{2.42}F_{0.2}$ gives rise to a change in the orientation of the magnetic moments on the Fe^{3+} ions by $90°$, which align in the a/b-plane in $15R-BaFeO_2F$ and $15R-BaFeO_{2.27}F_{0.5}$ compared to parallel to the c-axis in $15R-BaFeO_{2.42}F_{0.2}$ [16]. This demonstrates that small changes in structure and composition can have a significant impact on the compound's magnetic properties of these materials. $15R-BaFeO_2F$ was shown to be a very robust antiferromagnet with a Néel temperature between 300 and 400 °C and the magnetic structure is in good agreement with that expected from the GKA rules [51].

Acknowledgments

References

[1] G. Deng, Y. Chen, M. Tao, C. Wu, X. Shen, H. Yang, Electrochim. Acta 54 (2009) 3910–3914.
[2] P.A. Murade, V.S. Sangawar, G.N. Chaudhari, V.D. Kapse, A.U. Bajpeyee, Curr. Appl. Phys. 11 (2011) 451–456.
[3] L. Nalbandian, A. Evdou, V. Zaspalis, Int. J. Hydrogen Energy 34 (2009) 7162–7172.
[4] I. Gil de Muro, M. Insausti, L. Lezama, T. Rojo, J. Solid State Chem. 178 (2005) 1712–1719.
[5] N. Hayashi, T. Yamamoto, H. Kageyama, M. Nishi, Y. Watanabe, T. Kawakami, Y. Matsushita, A. Fujimori, M. Takano, Angew. Chem. Int. Ed. 50 (2011) 12547–12550.
[6] F. Iga, Y. Nishihara, T. Katayama, K. Murata, Y. Takeda, J. Magn. Magn. Mater. 104–107 (Part 3) (1992) 1973–1975.
[7] Y. Takeda, M. Shimada, F. Kanamaru, M. Koizumi, N. Yamamoto, Mater. Res. Bull. 9 (1974) 537–543.
[8] U. Müller, Anorganische Strukturchemie, B.G. Teubner Verlag, Wiesbaden, 2004.
[9] J.P. Hodges, S. Short, J.D. Jorgensen, X. Xiong, B. Dabrowski, S.M. Mini, C. W. Kimball, J. Solid State Chem. 151 (2000) 190–209.
[10] K. Yamaura, H.W. Zandbergen, K. Abe, R.J. Cava, J. Solid State Chem. 146 (1999) 96–102.
[11] J.M. Gonzalez-Calbet, M. Parras, M. Vallet-Regi, J.C. Grenier, J. Solid State Chem. 86 (1990) 149–159.
[12] K. Mori, T. Kamiyama, H. Kobayashi, K. Itoh, T. Otomo, S. Ikeda, Phys. B: Condens. Matter 329–333 (Part 2) (2003) 807–808.
[13] K. Mori, T. Kamiyama, H. Kobayashi, T. Otomo, K. Nishiyama, M. Sugiyama, K. Itoh, T. Fukunaga, S. Ikeda, J. Appl. Crystallogr. 40 (2007) s501–s505.
[14] J.C. Grenier, A. Wattiaux, M. Pouchard, P. Hagenmuller, M. Parras, M. Vallet, J. Calbet, M.A. Alario-Franco, J. Solid State Chem. 80 (1989) 6–11.
[15] M. Sturza, S. Daviero-Minaud, H. Kabbour, O. Gardoll, O. Mentré, Chem. Mater. 22 (2010) 6726–6735.
[16] M. Sturza, H. Kabbour, S. Daviero-Minaud, D. Filimonov, K. Pokholok, N. Tiercelin, F. Porcher, L. Aldon, O. Mentre, J. Am. Chem. Soc. 133 (2011) 10901–10909.
[17] V.M. Goldschmidt, Naturwissenschaften 14 (1926) 477.
[18] M. Parras, M. Vallet-Regi, J.M. Gonzalez-Calbet, M.A. Alario-Franco, J.C. Grenier, P. Hagenmuller, Mater. Res. Bull. 22 (1987) 1413–1419.
[19] K.G. Sanjaya Ranmohotti, E. Josepha, J. Choi, J. Zhang, J.B. Wiley, Adv. Mater. 23 (2011) 442–460.
[20] M.M. Kuklja, Y.A. Mastrikov, B. Jansang, E.A. Kotomin, J. Phys. Chem. C 116 (2012) 18605–18611.
[21] M. Sturza, S. Daviero-Minaud, M. Huvé, N. Renaut, N. Tiercelin, O. Mentré, Inorg. Chem. 50 (2011) 12499–12507.
[22] P.R. Slater, J. Fluorine Chem. 117 (2002) 43–45.
[23] P.R. Slater, J.P. Hodges, M.G. Francesconi, P.P. Edwards, C. Greaves, I. Gameson, M. Slaski, Physica C 253 (1995) 16–22.
[24] M. Al-Mamouri, P.P. Edwards, C. Greaves, M. Slaski, Nature 369 (1994) 382–384.
[25] A.M. Abakumov, J. Hadermann, G. Van Tendeloo, R.V. Shpanchenko, P. N. Oleinikov, E.V. Antipov, J. Solid State Chem. 142 (1999) 440–450.
[26] R. Heap, P.R. Slater, F.J. Berry, O. Helgason, A.J. Wright, Solid State Commun. 141 (2007) 467–470.
[27] F.J. Berry, F.C. Coomer, C. Hancock, Ö. Helgason, E.A. Moore, P.R. Slater, A. J. Wright, M.F. Thomas, J. Solid State Chem. 184 (2011) 1361–1366.
[28] F.J. Berry, X. Ren, R. Heap, P. Slater, M.F. Thomas, Solid State Commun. 134 (2005) 621–624.
[29] F.J. Berry, R. Heap, Ö. Helgason, E.A. Moore, S. Shim, P.R. Slater, M.F. Thomas, J. Phys.: Condens. Matter 20 (2008) 215207.
[30] Ö. Helgason, Hyperfine Interact. 184 (2008) 143–146.
[31] O. Clemens, R. Haberkorn, P.R. Slater, H.P. Beck, Solid State Sci. 12 (2010) 1455–1463.
[32] F.J. Berry, X. Ren, R. Heap, P. Slater, M.F. Thomas, J. Phys. Chem. Solids 69 (2008) 2032–2036.
[33] O. Clemens, M. Kuhn, R. Haberkorn, J. Solid State Chem. 184 (2011) 2870–2876.
[34] O. Clemens, A.J. Wright, F.J. Berry, R.I. Smith, P.R. Slater, J. Solid State Chem. 198 (2013) 262–269.
[35] M. Anji Reddy, M. Fichtner, J. Mater. Chem. 21 (2011) 17059–17062.
[36] O. Clemens, P.R. Slater, Rev. Inorg. Chem. http://dx.doi.org/10.1515/revic-2013-0002 (2013).
[37] H.M. Rietveld, Acta Crystallogr. 22 (1967) 151–152.
[38] H.M. Rietveld, J. Appl. Crystallogr. 2 (1969) 65–71.
[39] Topas V4.2, General profile and structure analysis software for powder diffraction data, User's Manual, Bruker AXS, Karlsruhe, (2008).
[40] R.W. Cheary, A.A. Coelho, J.P. Cline, J. Res. Natl. Inst. Stand. Technol. 109 (2004) 1–25.
[41] A.C. Larson, R.B. Von Dreele, Los Alamos National Laboratory Report LAUR (1994) pp. 86–748.
[42] B.H. Toby, J. Appl. Crystallogr. 34 (2001) 210–213.
[43] S.J. Clark, M.D. Segall, C.J. Pickard, P.J. Hasnip, M.J. Probert, K. Refson, M. C. Payne, Z. Kristallogr. 220 (2005) 567–570.
[44] J.P. Perdew, K. Burke, M. Ernzerhof, Phys. Rev. Lett. 77 (1996) 3865.
[45] J. Akimoto, Y. Gotoh, Y. Oosawa, Acta Crystallogr. 50 (1994) 160–161.
[46] R.D. Shannon, Acta Crystallogr. A 32 (1976) 751–767.
[47] E. Sullivan, C. Greaves, Mater. Res. Bull. 47 (2012) 2541–2546.
[48] S.A. Ivanov, S.G. Eriksson, J. Erikssen, R. Tellgren, H. Rundlof, Mater. Res. Bull. 39 (2004) 615–628.
[49] N.A. Jordan, P.D. Battle, J. Sloan, P. Manuel, S. Kilcoyne, J. Mater. Chem. 13 (2003) 2617–2625.
[50] E.H. Kisi, C.J. Howard, Applications of Neutron Powder Diffraction, Oxford University Press, New York, 2008.
[51] J.M.D. Coey, Magnetism and Magnetic Materials, Cambridge University Press, Cambridge, 2009.
[52] M. Schmidt, S.J. Campbell, J. Solid State Chem. 156 (2001) 292–304.